Purdue University
Purdue e-Pubs

School of Aeronautics and Astronautics Faculty Publications | School of Aeronautics and Astronautics

2007

Experimental and Computational Studies of Temperature Gradient Driven Molecular Transport in Gas Flows through Nano/Micro-Scale Channels

Yen-Lin Han
University of Southern California, yenlinha@usc.edu

Alina A. Alexeenko
Purdue University - Main Campus, alexeenk@purdue.edu

Marcus Young
Edwards Air Force Base

Eric Phillip Muntz
University of Southern California

Follow this and additional works at: http://docs.lib.purdue.edu/aaepubs

 Part of the Engineering Commons

Recommended Citation

Han, Yen-Lin; Alexeenko, Alina A.; Young, Marcus; and Muntz, Eric Phillip, "Experimental and Computational Studies of Temperature Gradient Driven Molecular Transport in Gas Flows through Nano/Micro-Scale Channels" (2007). *School of Aeronautics and Astronautics Faculty Publications.* Paper 5.
http://dx.doi.org/10.1080/15567260701337209

This document has been made available through Purdue e-Pubs, a service of the Purdue University Libraries. Please contact epubs@purdue.edu for additional information.

Experimental and Computational Studies of Temperature Gradient Driven Molecular Transport in Gas Flows through Nano/Micro-Scale Channels

Yen-Lin Han*,#, Alina Alexeenko**, Marcus Young***, Eric Phillip Muntz*

* Department of Aerospace and Mechanical engineering, University of Southern California, Los Angeles, CA 90089, USA

** School of Aeronautics and Astronautics, Purdue University, West Lafayette, IN 47907, USA

*** United States Air Force Research Laboratory, Edwards Air Force Base, CA 93524, USA

Abstract:

Studies at the University of Southern California have shown that an unconventional solid-state device, the Knudsen Compressor, can be operated as a micro-scale pump or compressor. The critical components of Knudsen Compressors are gas transport membranes, which can be formed from porous materials or densely packed parallel arrays of channels. An applied temperature gradient across a transport membrane creates a thermal creep pumping action. Experimental and computational techniques that have been developed for the investigations will be discussed. Experimental studies of membranes formed from machined aerogels, activated by radiant heating, have been used to investigate thermal creep flows. In computational studies several approaches have been employed: the direct simulation Monte Carlo (DSMC) method, and discrete ordinate solutions of the ellipsoidal statistical (ES) and Bhatnagar-Gross-Krook (BGK) kinetic models. Beyond the study of Knudsen Compressor performance, techniques discussed in this paper could be used to characterize the properties of gas flows in nano/micro-scale channels.

1. Introduction

Micro/meso-scale gas pumps or compressors are in demand for integration with other micro/meso-scale instruments [1]-[5] to form complete miniaturized systems. Many issues have been encountered in attempting to shrink full-scale conventional pumps successfully to micro/meso-

To whom correspondence should be addressed. yenlinha@usc.edu

scales [6]. The main difficulties are the required small manufacturing tolerances, the uncertainties associated with using supplementary fluids such as pump oil, thermal inefficiency, and short lifetime due to wear resulting from sliding friction. Unlike most conventional pumps, the Knudsen Compressor, a solid-state pump/compressor based on the gas kinetic phenomena of thermal transpiration and thermal creep, requires no moving parts or supplementary pumping fluids.

In 1910, Knudsen reported on the first multistage thermal transpiration pump, which successfully achieved a pressure increase of a factor of ten [7][8]. A series of ten capillary segments formed in a glass tube, along with Bunsen burners to provide temperature gradients across the capillary segments, were used in Knudsen's original experiments to demonstrate a thermal transpiration cascade. Restricted by the size of the capillary segments, the thermal transpiration could only be demonstrated at low pressures. Also, the thermal conductivity of glass or other porous materials at that time was relatively high, so the efficiency of the pumping process was low. Modern membrane materials with smaller channel sizes and extremely low thermal conductivity, such as aerogel, significantly improve a Knudsen Compressor's performance compared to Knudsen's 1910 investigations.

Based on Knudsen's original design, Pham-Van-Diep et al [9] suggested a modern version of the Knudsen Compressor in 1994. Vargo later demonstrated it using aerogel as the Knudsen Compressor membrane [10][11]. Performance analysis of the Knudsen Compressor has shown that it is most efficient if operated in the transitional flow region [12]. Using aerogel membranes, the micro/meso-scale Knudsen Compressor has successfully performed operations at atmospheric pressure down to 10s of mTorr at the University of Southern California [13]-[16].

1.1 History of Thermal Transpiration/Creep

Therma1 transpiration was originally investigated experimentally by Osborne Reyno1ds [17] in 1880, based on earlier experimental observations from 1831 to 1863 by Graham [18]. It was subsequently investigated by Knudsen [7] [8] and Gaede [19] among others and has been a subject of attention up to the present. Thermal transpiration is of course inextricably entwined with

isothermal molecular capillary flows. Chemists, nuclear scientists and applied mathematicians have all found reason to study capillary flows. Clausing [20] for instance was interested because transient molecular flow through a capillary channel gave a measure of the average dwell time of molecules in the adsorbed layer on the capillary's surface. Weber [21] in 1932 and later Liang [22] in 1951 developed semi-empirical expressions for gaseous diffusion in porous media. More recently (1961-1963) Evans, Watson and Mason [23] developed a mostly analytical "dusty gas" model for diffusion and thermal transpiration in porous media. At about the same time, beginning with Takao [24] in 1960 and shortly thereafter by Cercignani [25] in 1963, modern analyses of transitional Poiseuille flow have had an active history. Ferziger [26], Sone [27], Loyalka [28], and Cercignani [29] studied the transitional flow problem in capillaries during the late 1960's. In 1966 Miller and Buice [30] developed free molecule flow results for thermal transpiration in capillaries with velocity dependent surface scattering. Loyalka [31] used the Bhatnagar-Gross-Krook model of the Boltzmann equation to develop expressions of the transitional flow coefficients for thermal transpiration in 1969. Since that time there has been a steady stream of papers on transitional Poiseuille and thermal transpiration flows. Principally these have been from Loyalka and his colleagues at the University of Missouri [32], Porodnov and his colleagues at the Urals Polytechnic Institute [33]-[35], Sone and his colleagues at Kyoto University [36][37] and several recent papers by Sharipov [38]-[41] at both the Urals State University and the Federal University of Parana.

The flow through very small capillaries (~ 100 nm) has been the subject of attention from both the nuclear and chemistry communities [23][34]. Recently, because of their availability, micromachined channels with minimum dimensions down to 100 nm have been studied [42][43]. Somewhat larger minimum dimension micromechanical channels have been investigated by Breuer and his group [43]. These studies have raised interesting issues which have been looked at before, but in geometrically less well defined situations [44].

In parallel with the ability to produce well defined, 100 nm and smaller flow channels V.D. Borman, S. Yu. Krylov and their associates at the Engineering Physics Institute (Moscow) have,

beginning in 1986, developed a theory of molecular gas flow in small channels that self-consistently accounts for the dynamics of molecules and phonons [45]-[47]. Since 1990 collaboration of Borman and Krylov with Beenakker, Hermans and Hoogeveen at Leiden University has extended the interpretation of this work to sub-nanometer channel flows [48]-[50]. There have been several very recent numerical and analytical studies on nano-scale channel flow phenomena [51][52]. However, in well-defined nanometer to sub-nanometer flow channels, no experimental studies have yet convincingly investigated the complex, physical characteristics accompanying either temperature driven or pressure driven flows.

1.2 Thermal Creep Flow

Knudsen's view of thermal creep flow is illustrated in Figure 1. Thermal creep is used to describe what occurs in transitional rarefied flows, primarily along walls with a superimposed wall surface temperature gradient. Substantially diffuse and thermally accommodated reflections are required at the surface for thermal creep to be significant.

As indicated in Figure 1, thermal creep flow is from the cold end of a tube towards the hot end. For free molecular flow, thermal creep flow will fill the entire tube, becoming thermal transpiration. In the case of transitional flow, the thermal creep occurs closer to the tube's walls. As a consequence of the cold to hot flow a pressure difference between the hot and cold ends can be established a pressure return flow will occur, partially or completely balancing the thermal creep flow. Thus, thermal creep can produce both a net gas flow and a pressure difference, which are the requirements for a pump.

1.3 Theoretical Flow Model for a Single Stage Knudsen Compressor

A single stage of a Knudsen Compressor is illustrated in Figure 2 as suggested by Muntz et al [12]. Each stage has a membrane section, where temperature increases, causing the pressure increases due to the rarefied gas phenomena of thermal creep or thermal transpiration. Following the membrane section, there is a connector section with a significantly larger radius than the individual capillaries. Under normal operation, the connector section operates with the gas flow closer to the

continuum regime, so that the pressure is approximately constant while the gas temperature is lowered to $T_{L,i}$, the gas temperature entering the stage.

A Knudsen Compressor optimization analysis [12] was conducted based on flow coefficients calculated from the linearized Boltzmann's equation for transitional flows through an infinite capillary [37]. Two flow coefficients, the thermally driven flow coefficient and the pressure driven return flow coefficient, are available as functions of Knudsen numbers [37]. Based on the operating Knudsen number in the flow channel, both mass flow and the pressure change can be obtained.

The mass flow ($\dot{M}$) through a capillary tube of length L_x, assuming small temperature and pressure gradients, can be written as

$$\dot{M} = p_{avg}\sqrt{\frac{m}{2kT_{avg}}}A\left(\frac{L_r}{L_x}\frac{\Delta T}{T_{avg}}Q_T - \frac{L_r}{L_x}\frac{\Delta p}{p_{avg}}Q_P\right). \tag{1}$$

Here Δp is the pressure difference, p_{avg} is the average pressure in the capillary tube, ΔT is the temperature difference, T_{avg} is the average temperature in the capillary tube, Q_T is the thermally driven flow coefficient, Q_P is the pressure driven return flow coefficient, A is the capillary's cross-sectional area, L_r is the radius of the capillary tube, L_x is the length of the capillary tube, m is the molecular mass of the gas, and k is Boltzmann's constant. Physically, the two competing flows illustrated in Figure 2 (the thermally driven flow that is described by Q_T, and the pressure driven flow that is described by Q_P) form the net gas flow.

When Eq. (1) is set equal to zero, the thermally driven upflow is exactly balanced by the pressure driven return flow. In this situation, the pressure change Δp is at its maximum value designated as Δp_{max}, and Eq. (1) reduces to

$$\frac{\Delta p_{\max}}{p_{avg,\max}} = \frac{\Delta T}{T_{avg}}\frac{Q_T}{Q_P}. \tag{2}$$

Due to the relatively small length to diameter ratio in the connector section, it is not completely accurate to apply the linearized analysis of transitional flow to the connector. The coefficients were developed under the assumption of infinite tube length. Neverthelessan approximation is useful, it is

convenient to express the pressure drop due to thermal creep in the connector section opposite to the pressure increase in the membrane section using the linearized approximation [12]. Assume that the gas temperature at the connector section's outlet returns to the stage's inlet temperature. Also assume that the average pressure in the connector section is the same as in the capillary section. The ratio of the maximum pressure change for the entire Knudsen Compressor stage to the maximum average pressure at $\dot{M} = 0$ is

$$\frac{(\Delta p_{\max})_T}{p_{avg,\max}} = \frac{|\Delta T|}{T_{avg}}\left[\frac{Q_T}{Q_P} - \frac{Q_{T,C}}{Q_{P,C}}\right]. \tag{3}$$

The subscript *C* indicates the connector section, $|\Delta T|$ is the temperature change in both the capillary section and connector section. The flow coefficients provide basic theoretical predictions of the flow phenomena through the membrane channels and the connector section of a Knudsen Compressor. Comparisons of the flow coefficient prediction and the experimental and simulation results will be presented in later sections.

1.4 Thermally Driven Flows in Sub-Nano/Nano-Scale Size Channels

At channel sizes of several nanometers and below, the molecules in a flow channel spend a significant amount of time interacting with the walls' attractive force fields, thus increasing the near-wall number densities. One result can be an increase in the thermally driven flow above the classical thermal gradient driven transpiration. Another physical effect that may become noticeable for nanometer size thermal transpiration channels is a coupling of the gas flows near the walls to the phonon flux in the wall material [45][49][50]. The coupling occurs when the mean travel distance of the molecules along the tube axis between collisions with the channel's wall is on the order of the phonon mean free path in the solid, leading to an enhancement of the collisional coupling between phonon and molecule flows [45][49]. Phonon-molecule drag will be most pronounced for crystalline structures and may not be seen in random amorphous materials such as aerogel. Drag due to phonon-molecule coupling could counteract the potential for the increased efficiency mentioned above for thermally driven flows due to near wall gas density increases. For low enough

temperatures, which enhance the coupling, the phonon drag could even drive the flow in the opposite direction.

There are also two quantum effects predicted for flows in nanometer-size flow channels at room temperature [50]. In certain cases the zero point energy of the molecules can overcompensate for the attractive potential energy of the well formed by the interaction of a molecule and the capillary's walls. In this case, the number of molecules in the capillary is reduced by a Boltzmann factor, leading to a screening effect based on their deBroglie wavelength in the radial direction and the strength of their interaction with the walls. The other quantum effect that has been predicted to become important in nano-scale flows occurs when the first molecular excited state in the channel is high compared to the thermal energy of the molecules. If this condition is met almost all of the gas will be in the ground state and thus it will behave as a one-dimensional gas. All of these effects increase the complexity of the interactions between the physical processes that influence the flows.

The maximum normalized steady state pressure difference that can be produced divided by the normalized temperature difference applied to a thermal transpiration channel is known as the thermomolecular pressure difference ($TMPD=(\Delta p_{max}/p_{avg})/(\Delta T/T_{avg})$). The theoretical analysis based on flow coefficients for transpiration membranes with channel radii smaller than several nanometers, will require modified expressions for the thermally driven upflows and the pressure return flows, and an additional term for molecule-phonon coupling.

For normal thermal transpiration/creep flows, there are two parameters that determine the TMPD; the gas Knudsen number and the accommodation coefficient of the channel's wall. As the capillary radius becomes on the order of several nanometers it is predicted that the mean temperature of the tube will also become important. Once the channel radius has been shrunk to a size such that a molecule spends nearly all of its time interacting with the wall, the flow becomes two-dimensional (2D) and new temperature effects become important. At high temperatures the TMPD asymptotes to ½. As the temperature is decreased the increased interaction time with the wall makes the thermal transpiration effect more efficient. As the mean temperature decreases even

further the phonon drag due to molecule-phonon coupling may become relatively more important. This effect is most pronounced when the mean free path of the gas-surface interaction is similar to the mean free path of the phonon-phonon collisions in the solid lattice. Beenakker et al. have shown that the TMPD maximum occurs at roughly 240K for gases like Ar and N_2 [49][50]. They have also shown that the crossover to negative TMPD, driven by molecule-phonon coupling, occurs at roughly 140-180K. For instance, if these temperature effects on TMPD were found experimentally for the nonideal flow channel structure in aerogel, then it might be possible to adjust the mean temperature of the Knudsen Compressor to operate at the TMPD maximum.

Figure 3 shows the TMPD that would occur for: the case of the thermal transpiration effect (TMPDth), the case of the phonon drag effect (TMPDph), and the total TMPD for CO_2 on C with a channel diameter of 4nm. The total TMPD is the difference between the two TMPDs. The TMPD asymptotes to a value near 0.5 at high temperatures. The phonon drag causes the TMPDph to increase negatively as the temperature decreases. The net TMPD goes negative at slightly over 200K when the effect of increased number densities in the potential wells results in a continuous increase in TMPDth as the temperature decreases. It does appear, however, that there is a TMPD maximum around 400K and the crossover to negative TMPD at about 225K. It is difficult to make any definitive conclusions based on this approximate analysis for the phonon drag effect. It is important to note that phonon drag effects may become important at low temperatures and at pore sizes below 5nm.

The increased importance of the gas-surface interactions in pores with flow channel diameters under 5nm requires a gas surface interaction potential model. Beenakker et al's previous analyses included different interaction potentials for different cylindrical channel sizes [49][50]. For larger channel diameters, where the interaction potentials from the different sides of the tube do not overlap significantly, an interaction potential is defined with a range, L, from the channel wall and a depth, V. Smaller pores where the interaction potentials from the opposite sides of the channel overlap significantly are modeled as circular square well potentials. Figure 4 illustrates the range of

possible parameters (channel diameter in sub-nanomemeter range and in nanometer range) for the two model potentials compared to the corresponding cylindrical channel van der Waals potential for N_2 on SiO_2.

It is clear that both potential well models are approximate when compared to the van der Waals potential, which in itself is approximate, and that calculations based on these models are only qualitative until they can be validated experimentally. In the examples presented in figure 4, and referring to the van der Waals potentials, the 1 nm diameter channel exhibits a potential well filling the entire channel, while for the 2 nm diameter channel, the center portion is almost free of wall attraction. In this case, the quantum effects described earlier would only be of possible significance for diameters significantly less than 1 nm. On the other hand, the effect of increased near-wall densities would still be important for the 2 nm diameter channel.

1.5 Nano-Scale Pore Condensation

At small flow channel radii increased gas adsorption can occur on the flow channel surfaces [47]. This effect can lead to flow channel blockage through gas condensation. It also may lead to flow enhancement in pressure driven flows [47]. The increased adsorption in the capillaries is due to the decreased vapor pressure from the high curvature of the small channels and is related to the increased gas surface potential well depths described earlier. The effects of pore condensation on membrane transport is an important subject, because of broad interest in the chemical physics community it is of a scope that makes it impossible to include in the present discussion.

2. Experimental studies of temperature driven flow phenomena

Using aerogel for Knudsen Compressor membranes, many experimental studies of temperature driven flows have been conducted. Aerogel has very low overall thermal conductivity (~ 20 mW/m-K), and mean pore sizes in the 10s of nm range [53]. The low thermal conductivity offers the advantage of maintaining a temperature difference across the membrane with minimum energy consumption. Nominal aerogel membranes can be efficient operating near atmospheric pressure down to 30 Pa. At lower pressures, channel sizes significantly larger than 20 nm are required. One

solution is to machine optimally sized channels in aerogel membranes. The advantages of aerogel's extremely low thermal conductivity and significantly higher flow conductances can be realized.

Both resistive and radiant heating techniques for aerogel membranes have been studied [14][15][16]. Similar experimental procedures were used. The mechanically machined aerogel membrane is used as an example here. In these experiments, the radiant heating technique was adopted. An 8% carbon doping fraction aerogel with density of 80 mg/cm^3 was used, based on results from an earlier study [15].

Several mechanically machined, carbon doped aerogel membranes have been prepared. Figures 5 & 6 show close-up views of the mechanically machined aerogel membrane. The aerogel piece is sealed on the aluminum thermal guard by TorrSeal®. Before the machining process, the stage was tested at atmospheric pressure to verify the efficacy of the side sealing. Under a microscope, no major cracks can be observed in the drilled membranes. Also, the circular shape of the capillaries is evident. The capillaries shown in Figure 5 are centered to the holes in the aluminum thermal guard, which currently are 0.5 mm in diameter. There are a total of 99 capillaries through the aerogel membrane, which is the same as the number of holes in the aluminum thermal guard. The open area of the membrane is easily calculated. Other than drilling capillaries, aerogel membranes can be mechanically machined into several rectangular channels by following preparation steps similar to those for the capillaries. Figures 6 presents an image of a membrane with mechanically machined rectangular channels. The corresponding aluminum thermal guard has six rectangular channels, each 0.5 mm in height and 5 mm in width.

Despite the different shapes of flow channels, both capillary and rectangular channel membranes can be used with the same experimental setup and procedures. The purpose of undertaking these experiments was to characterize the performance of a single, mechanically channeled, carbon doped aerogel membrane. For each experiment a new membrane, which was machined after being sealed to the top of an aluminum thermal guard, was mounted in a single stage Knudsen Compressor setup. The cross-sectional view of a basic, radiantly driven single stage

Knudsen compressor, is shown in Figure 7. The flow directions are shown by arrows. The desired experimental data included the pressures in both hot side and cold side chambers, the differential pressures across the single Knudsen Compressor stage, and in some cases temperatures of both the hot and cold sides of the membranes.

The experiment was set up as a closed system as illustrated in Figure 8, which has some similarity with an earlier apparatus used by Porodnov et al [34][54]. Thermocouples (J type) were used for the temperature measurements. The radiantly driven single stage Knudsen Compressor was connected to two volumes, hot side and cold side, with ¼ inch diameter tubes. The hot side volume is 1.9×10^{-3} m^3 and the cold side volume is 1.2×10^{-2} m^3. A 200 mTorr differential Baratron (MKS Type 223, reading error of ±0.3% of 200 mTorr) pressure gauge was connected to the volumes through different outlets to monitor directly the pressure changes. MicroPirani gauges (MKS A900 series, reading error of 5%) were connected to the cold side and hot side volumes in order to record the absolute pressures in each chamber. A toggle valve (denoted as short circuit valve) was connected between the cold side volume and the hot side volume to provide a "short circuit" for the two gas flows between the chambers. The light source used in these experiments was a Halogen lamp (Electrix 50W/12V). In order to increase the heat flux going into the membrane, a focusing lens was used to concentrate the light generated by the source on the membrane area. The incident flux (mW/cm^2) was measured by a radiant power meter (Oriel 70260) before taking experimental data.

With the short circuit valve opened, the volumes of both hot and cold sides were pumped down to the desired operating pressure, for example, around 133 Pa (1 Torr) for the mechanically channeled aerogel membrane with 210 μm diameter capillaries. After the short circuit valve was closed, the pressure on both sides was allowed to settle to equilibrium. The Halogen lamp was then turned on, and LabVIEW codes recorded Δp (pressure difference) from the differential Baratron and p_L, p_H (absolute pressure of the cold side and hot side respectively) from the MicroPirani gauges. After several hundred seconds (time scale depending on the size of the flow channels) a maximum

Δp was reached within the experimental scatter. The Halogen lamp was then shut down to record the vent-up response of the pump, by which the flow was driven through the membrane by the pressure difference. The readings from the MicroPirani gauges and the differential Baratron were recorded by LabVIEW for the vent-up process as well.

A typical time trace of experimental data is shown in Figure 9. The light source was turned on at t = 0 sec, and was turned off at t = 500 sec. Note that in the figures, p_c is denoted as pc and Δp is denoted as dp.

Figure 10 shows an example curve fit, obtained by varying $\tilde{\tau}$ and Δp_{max} using

$$\Delta p(t) = \Delta p_{\max}(1 - e^{-t/\tilde{\tau}}). \tag{4}$$

The characteristic time constant $\tilde{\tau}$ is given by

$$\tilde{\tau} = \frac{1}{C_M\left(\frac{1}{V_H} + \frac{1}{V_L}\right)}. \tag{5}$$

Here C_M is the membrane conductance. V_H and V_L are the hot side and cold side volumes respectively.

Compared to the experimental data, the best curve fit was determined when the mean square error was minimized. As an example, for the curve fit shown in Figure 10, $\tilde{\tau}$ was iterated to be 25.4 seconds and Δp_{max} = 3.4 Pa at an operating pressure close to 136 Pa. In the figure, Δp is noted as dp and dpfit represents the value calculated by Eq. (4) for a given $\tilde{\tau}$. It is essentially a perfect fit which implies an effectively instantaneous achievement of quasi-steady state flow condition at all times during the run, this assumption plus molecule conservation were used to derive Eq (4).

The membrane conductance analysis answered the following question, whether significant numbers of gas molecules will pass through the nominal aerogel part of the machined membrane? The open area fraction of the machined rectangular channel membrane is 15%, and the capillary

membrane is about 5% nominal aerogel. Pressure difference builds up more quickly due to flow through the machined channels. In general, the time constant to reach equilibrium for the nominal aerogel without machined channels is about 100 times longer than that for machined aerogel membranes. The nominal aerogel membrane's conductance is then 2 orders of magnitude less than the machined channel membrane's conductance. Due to the significant difference in conductance and time constant, practically all the gas molecules are transported through the machined channels rather than the nominal aerogel channels.

Corresponding to each operating pressure, p_{avg}, the maximum pressure difference, Δp_{max}, shown in the time traces (Figures 9, 10) has been recorded and the ratio of $\Delta p_{max}/p_{avg}$ was plotted for the membranes with different capillary sizes. Using the membrane temperatures calculated from the temperature model reported by Young [15], the predicted maximum pressure differences, with and without taking into account possible reverse thermal creep effects, can be calculated and are shown as the model values in Figure 11. In this case, representative experimental results from the 380 μm diameter capillary membrane are shown. The model predicted surface temperature of a 1 cm^2 aerogel membrane is 377 K at around 13.3 Pa for an incident flux of 125 mW/cm^2. In all cases, the same trend was observed. Using a 5.0 mm (LR,c = 5mm in Figure 11) characteristic dimension for the connector section, the discrepancy between the model and the experimental data appeared when flows in the connector section entered be in the transitional regime. The connector section is then subject to rarefaction phenomena, such as "reverse" thermal creep and related thermally induced internal flow. It is important to be able to account for these effects.

If the "reverse" thermal creep flow is taken into account, using a 5.0 mm characteristic dimension for the connector section, the corresponding predicted maximum pressure differences are shown as triangles in Figure 11. As can be seen when the "reverse" thermal creep effect has been taken into account in the model, the discrepancy becomes smaller. All other membranes exhibited the same characteristics. "Reverse" thermal creep flows were certainly seen from these experiments; however, the effect was significantly larger than predicted.

One reason for the discrepancy between the model and experimental data comes from the geometry of the current single stage design. Model predictions assumed that the connector section is a straight flow channel with a temperature gradient from its inlet temperature, T_H, to its outlet temperature, T_L. In the experimental setup, however, the connector section introduces three 90^o bends in the flow channel (Figure 7). Also, the temperature distribution is nothing like assumed in the model calculations. In Figure 12, only the aerogel surface is hot, all of the inner walls and the Plexiglas cover are at low temperatures. The relatively high Knudsen number in the connector section, and the geometric restrictions of the present design, likely introduce complex, "reverse" thermal creep induced internal circulation due to the temperature differences between the hot membrane surface and the cold connector walls.

The current temperature model neglects these effects, which, among other consequences, may cause higher heat loss through convection from the aerogel's surface. Hence the aerogel surface's predicted temperatures from the aforementioned model could be higher than temperature experienced in the experiments. These secondary flows are basically radiometer flow effects, such as one well known to occur in Crookes' Radiometer [54]-[59]. They have recently been studied by DSMC simulation techniques [36][60]-[65]. Although there are some practical computational cost limitations, simulations can be used to investigate the influence of reverse thermal creep. Both reverse thermal creep and thermal creep induced flows can usefully be simulated as discussed in the following section.

3. Simulations – DSMC, Elliptical Statistical and BGK:

The phenomenon of thermal transpiration arises due to the presence of significant temperature variations over length scales comparable to the mean free path of molecules. Computational studies of transpiration flows have to be based on a kinetic description of gas flows. The Kinetic Theory offers a framework for description of the temporal and spatial variation of the velocity distribution function of molecules due to the action of an external force, intermolecular collisions and collisions

of gas molecules with solid surfaces. The governing equation for the velocity distribution function of a dilute ideal gas is the Boltzmann equation:

$$\frac{\partial f}{\partial t} + \vec{v}\frac{\partial f}{\partial \vec{x}} + \vec{F}\frac{\partial f}{\partial \vec{v}} = \int_{-\infty}^{+\infty} (f' f'_1 - f\ f_1) v_r \frac{\partial \sigma}{\partial \Omega} d\Omega d\vec{v}_1 \quad . \tag{6}$$

Here v_r is the relative speed, f is the velocity distribution function, ' denotes the values of the distribution function for post-collisional velocities, and $\frac{\partial \sigma}{\partial \Omega}$ is the differential collision cross-section.

In general, a direct numerical solution of this integro-differential equation is an arduous task due to the complicated form of the multidimensional collision integral in the right hand side. The direct simulation Monte Carlo (DSMC) method [66] is a stochastic approach for modeling gas flows in the rarefied regime, due to the same processes as described by the Boltzmann equation. The fundamental principle of the DSMC method is splitting of the continuous motion of molecules into two stages, free molecular flight and intermolecular collisions. The collisions are calculated based on molecular velocities only for representative simulated particles in close proximity to each other. For example, particles located in one cell of a computational mesh. The macroscopic parameters of the gas flow such as bulk velocity, temperature and density are obtained as time and volume averages of molecular properties such as mass, momentum and kinetic energy of the simulated particles.

Starting from the pioneering work by Bird [66] in the early 1960s, the direct simulation Monte Carlo (DSMC) method has evolved into a powerful numerical tool that provides accurate and efficient solutions to many important problems of rarefied gas dynamics. However, the computational cost of the DSMC method increases with decreasing Mach number. This is due to explicit time integration in the DSMC algorithm, and to larger sample sizes that are necessary to attain a reasonable signal-to-noise ratio for gas flows when the average bulk gas velocity is small compared to the molecules mean thermal speed. The thermal transpiration flows in the Knudsen

Compressor are characterized by extremely low flow speeds, on the order of m/s. Additionally, coordinate transformation in the physical space domain, that could greatly increase computational efficiency for high aspect-ratio transpiration membrane channel geometry, can not be implemented in a DSMC simulation. Therefore, an alternative deterministic computational approach was applied in this work. The numerical method is based on the solution of the approximate form of the Boltzmann equation known as the ellipsoidal statistical (ES) kinetic model:

$$\frac{\partial f}{\partial t} + \vec{v}\frac{\partial f}{\partial \vec{x}} + \vec{F}\frac{\partial f}{\partial \vec{v}} = \frac{f_0 - f}{\tau} \quad , \tag{7}$$

where τ is the mean collision time and f_o is the three-dimensional anisotropic Gaussian:

$$f_o(\vec{v}) = \frac{n}{\sqrt{(2\pi)^3 \det[\lambda_{ij}]}} \exp(-\varepsilon v'_i v'_j) \, , \tag{8}$$

and

$$\lambda_{ij} = \frac{1}{\Pr} RT\delta_{ij} + \frac{1 - 1/\Pr}{\rho} p_{ij} \, . \tag{9}$$

where Pr is the Prandtl number, ρ is the mass density, and p_{ij} is the pressure tensor. The ES model equation possesses the same collision invariants as the Boltzmann collision integral and satisfies the H-theorem. Moreover, the ES model allows two gas transport coefficients – viscosity and thermal conductivity – to be reproduced, unlike the BGK kinetic model that can only specify either one of them. In this work the discrete ordinate method was applied for numerical solution of the ES model kinetic equation for thermal transpiration flow in a two-dimensional channel. A Gauss-Hermite quadrature of order 16 and the three-eighths rule was used for numerical integration of the velocity distribution function in cylindrical coordinates. A second-order finite difference scheme was used for numerical solution of the resulting system of partial-differential equations to obtain the values of the velocity distribution functions at the quadratures' abscissa.

Figure 13 shows a comparison of the velocity profiles along the channel centerline as calculated by the three models (DSMC, ES and BGK) for thermal transpiration flow in a channel with; length-

to-height ratio (Lx/h) of 5, Knudsen number in the hot reservoir equal to 0.2, and the temperatures of the cold (left) and hot (right) chambers equal to 300 K (T_L) and 500 K (T_H), respectively. The flow shown in Figure 13 is driven by a temperature gradient only, due to upstream and downstream pressures that were defined to be equal in this particular case. This open flow situation with a non-zero mass flow is typical for the initial stages of a Knudsen Compressor's operation. The wall temperature changes linearly along the channel length and a fully-diffuse Maxwell model of gas-surface interaction is used in all three computational models.

All three methods predict a qualitatively similar flowfield with the gas velocity increasing in the channel along the temperature gradient as the temperature increases from the left chamber to the right one. However, the streamwise velocity magnitude inside the channel predicted by the BGK model is about 20% lower than that calculated by DSMC and ES. The transpiration velocity is underpredicted by the BGK model because it corresponds to a Prandtl number of 1, instead of the value of around 0.7 typical for diatomic gases at room temperature. This results in an effectively lower coefficient of heat conduction in the BGK solution and smaller values of thermal creep. The DSMC and ES solutions are in good quantitative agreement, with the difference between the two predictions being less than the statistical scatter of the DSMC results.

The influence of wall temperature distributions inside the channel on the gas flowfield and thermal transpiration flow rate have been studied in Ref. [67] using the ES, BGK and DSMC models. It was found that the reverse transpiration for the non-monotonic temperature distribution, which is typical for a radiantly heated carbon-doped aergogel membrane, results in significant degradation of mass throughput (by ~18 %) for the same temperature difference between the hot and cold containers.

3.1 Flow Structure of Thermal Creep

A qualitative description of thermal creep flow structure was suggested by Knudsen in the early 1900's and is illustrated in Fig. 1. In this work a computational study of the thermal creep flow has been carried out using the numerical solution of the ES model kinetic equation described above. The

flow system is closed, with a zero net mass flow between the cold and hot chambers. The thermolecular pressure difference has built up between the two containers. The flow field is thus typical of the steady state, no net flow condition of Knudsen Compressor operation.

Figures 14 and 15 show the calculated flow structure of a thermal creep flow between two chambers maintained at the temperatures of 300 and 500 K, respectively, and connected by a 2D channel with a length-to-height ratio of 5. The streamlines of the flow show that two clockwise vortices develop in the cold and hot chambers. The flow structure in the transpiration channel is in fact more complex than the qualitative picture drawn by Knudsen. The thermal creep flow in the direction of the temperature gradient occupies a significant portion of the channel cross-section whereas the return pressure-driven flow is confined to a small region near the centerline. Interestingly, the numerical solution indicates a presence of very slow return flow adjacent to the channel wall. The resulting vortex near the outlet corner is caused by the separation of the thermal creep flow due to the adverse pressure gradient. The presence of vortical structures in a transient thermal creep flow may significantly affect the overall mass flow rate in the Knudsen Compressor. Further numerical studies are necessary to elucidate the structure of thermal creep flow in the whole range of Knudsen number regimes and its dependence on the conduit and reservoir geometry.

Another important feature of rarefied gas flows driven by temperature gradients is the separation of pressure tensor components. As J. C. Maxwell explained: “when inequalities of temperature exist in a gas, the pressure at a given point is not the same in all direction, and that the difference between maximum and minimum pressure at a point may be of considerable magnitude when the density of the gas is small enough” [57]. Figure 16 shows the pressure tensor components calculated by the ES model kinetic equation solver for the thermal transpiration flow with the conditions described above. The difference between the pressures in the X, Y and Z directions is evident at the channel inlet and exit regions. Such a non-equilibrium behavior in a gas flow can only be captured by a kinetic numerical method.

3.2 DSMC Simulations Representing the Single Stage Knudsen Compressor

To investigate the influence of the 'reverse' thermal creep and the thermal creep induced internal flows in the experimental data discussed in sec. 2, several DSMC simulations have been conducted. The case presented here is a simplified single stage Knudsen Compressor mimicking the experimental single stage design as illustrated in Figure 17(a). As shown in Figure 17(b), the simplified stage has two chambers connected with a membrane flow channel in a two-dimensional flow domain.

To save simulation cost, a larger than typical temperature gradient was adopted in the simulations. The single membrane channel has a length to height ratio (Lx/h) of 5. Experimental temperature measurements of the Plexiglas cover show that the side walls remained cold even when the aerogel surface was hot. As shown in Figure 17, a step temperature profile is imposed along the aerogel surface in the simulation domain. Only a fraction of the wall was kept at a constant hot temperature, T_H, but the rest of the wall was kept at a constant cold temperature, T_L.

Figure 18 shows the streamlines from the simulation results. Due to a larger cell size, the resolution of the DSMC simulation is not enough to show the revere streamlines near the center of the membrane channel as indicated in Figures 14 and 15. Also, the wall temperature in the hot side chamber is very different from what was imposed in Figures 14 and 15. The flow patterns shown in Figures 14 and 15 are solely from the temperature gradient in the membrane section but in Figure 18, the complicated wall temperature distribution introduced in the hot side creates the internal flow circulation from the 'reverse' thermal creep. This result demonstrates a possible flow situation in the experimental setup but with a higher temperature ratio across the membrane channel section. Theoretical flow coefficients would not be able to predict such complex temperature driven flow.

4. Summary

Studies of Knudsen Compressors have led to in-depth investigations of micro/nano-scale temperature driven flow phenomena. An applied temperature gradient across a Knudsen

Compressor's transport membrane, which can be formed from materials with randomized flow channels (porous materials) to arrays of multiple individual flow channels, creates a thermal creep pumping action. Flow coefficients obtained from the linearized Boltzmann equation provide theoretical predictions of the transport mechanisms through the transpiration membrane. As flow channel size decreases to nano/subnano-scales, effects due to phonon coupling, surface force fields, mobile adsorbed gases, and pore condensation can be important.

Experimental and computational techniques that have been developed for the investigations were discussed. Experimental data on machined aerogel membranes indicated the existence of complex 'reverse' thermal creep flow in the connector section of the Knudsen Compressor. The flow coefficients could not accurately predict the flow situation, in part due to the complicated geometry and wall temperature distribution of the experimental single stage Knudsen Compressor's connector section. Simulations were the choice to assist in developing further understanding of such complex flow phenomena.

In the computational studies several approaches have been employed: the direct simulation Monte Carlo (DSMC) method; two discrete ordinate solutions for the ellipsoidal statistical (ES) and the Bhatnagar-Gross-Krook (BGK) kinetic models. As an example, the influences of several wall temperature distributions within a membrane's flow channels were investigated. Results showed the mass flows were highly dependent on the temperature distributions in membrane channels. Also, the qualitative picture of the flow structure in a short transpiration channel is in fact considerably more complex than what proposed by Knudsen for a long channel. DSMC simulations mimicking the real single stage Knudsen Compressor design has confirmed qualitatively the internal circulation near the membrane channel outlet due to 'reverse' thermal creep.

A more complete quantitative understanding of the various internal flows remains to be developed through more extensive computations, using extensions of the techniques described in this paper. At first, the experiment design will be simplified to remove complicated flow geometries

in the connector section. Using the ES Kinetic model, it will be possible to undertake simulations that incorporate the experimental temperature ratios.

Beyond the study of Knudsen Compressor performance, experimental and simulation techniques discussed in this paper can be used to characterize the properties of a broad range of flow channels. With the rapidly changing state of the art for manufacturing very small, relatively well-defined flow channels from various materials, it can be anticipated that there will be significant advances in the experimental study of micro/nano/subnano-scale phenomena related to gas flows.

Nomenclature

A	cross-sectional area
b	width of a rectangular membrane channel
C_M	conductance through a membrane
f	the velocity distribution function
f_o	is the three-dimensional anisotropic Gaussian
h	height of a rectangular membrane channel
H	height of a rectangular membrane channel
k	Boltzmann's constant
Kn	Knudsen number
$Kn_{H/2}$	rectangular channel connector Knudsen number
$Kn_{h/2}$	rectangular channel membrane Knudsen number
Kn_r	capillary membrane Knudsen number
Kn_R	capillary connector Knudsen number
L_R	radius of the capillary connector tube
L_r	radius of the capillary membrane tube
L_X	length of the capillary connector tube
L_x	length of the capillary membrane tube

m	molecular mass
$\dot{M}$	mass flow
M_P	rectangular channel pressure driven flow coefficient
M_T	rectangular channel thermal driven flow coefficient
$p_{(i)}$	exit pressure of the *(i)*th stage
$p_{(i-1)}$	exit pressure of the *(i-1)*th stage
p_{avg}	average pressure
p_H	pressure of the hot chamber
p_{ij}	the pressure tensor
p_L	pressure of the cold chamber
Pr	Prandtl number,
Q_P	capillary pressure driven flow coefficient
Q_T	capillary thermal driven flow coefficient
T_{AVG}	average temperature
T_H	temperature of the hot chamber
T_L	temperature of the cold chamber
v_r	the relative speed
$\Delta p_{\max}$	pressure difference
$(\Delta p_{\max})_T$	total pressure gain through the *i*th stage
ΔT	temperature difference
λ	mean free path
ρ	the mass density
τ	is the mean collision time
$\tilde{\tau}$	characteristic time constant

$\frac{\partial\sigma}{\partial\Omega}$ the differential collision cross-section

References

1. M. Geear, and R.R.A. Syms, Monolithic MEMS Quadrupole Mass Spectrometers by Deep Silicon Etching, Journal of Microelectromechanical Systems, 14.5, pp.1156, 2005.
2. C.B. Freidhoff, R. M. Young, S. Sriram, T. T. Braggins, T. W. O'Keefe, J. D. Adam, H. C. Nathanson, R. R. A. Syms, T. J. Tate, and M. M. Ahmad, S. Taylor and J. Tunstall, Chemical Sensing Using Nonoptical Microelectromechanical Systems, Journal of Vacuum Science & Technology A, vol. 17 (4), pp. 2300-2307, 1999.
3. E. S. Kolesar, R.R. Reston, Review and Summary of a Silicon Micromachined Gas Chromatography System, IEEE Transactions on Components Packaging and Manufacturing Technology, Part B-Advanced Packaging, vol. 21 (4), pp. 324-328, 1998.
4. S.C. Terry, J.H. Jerman, and J. B. Angell, Gas-Chromatographic Air Analyzer Fabricated On A Silicon-Wafer, IEEE Trans. Electron Devices, vol. 26(12), pp. 1880 – 1886, 1979.
5. T.H.P. Chang, D.P. Kern, and M.A. McCord, L.P. Muray, A Scanning Tunneling Microscope Controlled Field-Emission Microprobe System, Journal of Vacuum Science & Technology B, vol. 9(2), pp.438-443, 1991.
6. E.P. Muntz, and S.E. Vargo, Micro Scale Vacuum Pumps, The MEMS Handbook, Ed. G. Gad-el-Hak, CRC Press, pp. 29_1-29_28, 2002.
7. M. Knudsen, Eine Revision der Gleichgewichtsbedingung der Gase. Thermische Molekularströmung, Annalen der Physik, vol. 336 (1), pp. 205-229, 1909.
8. M. Knudsen, Thermischer Molekulardruck der Gase in Röhren, Annalen der Physik, vol. 338 (16), pp. 1435-1448, 1910.

9. G. Pham-Van-Diep, P. Keeley, E. P. Muntz, and D. P. Weaver, A Micromechanical Knudsen Compressor, Rarefied Gas Dyanmics, Eds. J. Harvey and G. Lord, Oxford University Press, Oxford, pp.715-721, 1995.
10. S. E. Vargo, and E. P. Muntz, An Evaluation of a Multiple Stage Micromechanical Knudsen Compressor and Vacuum Pump, Rarefied Gas Dynamics, Ed. Ching Shen, Peking University Press, Beijing, pp. 995-1000, 1997.
11. S. E. Vargo, E.P. Muntz, G. R. Shiflett, and W.C. Tang, The Knudsen Compressor as a Micro and Macro Scale Vacuum Pump without Moving Parts or Fluids, Journal of Vacuum Science & Technology A, vol. 17, pp. 2308-2313, 1999.
12. E.P. Muntz, Y. Sone, K. Aoki, S. Vargo, and M. Young, Performance Analysis and Optimization Considerations for a Knudsen Compressor in Transitional Flow, Journal of Vacuum Science & Technology A, vol.1, pp. 214, 2002.
13. S. E. Vargo, and E. P. Muntz, Comparison of Experiment and Prediction for Transitional Flow in a Single Stage Micromechanical Knudsen Compressor, Rarefied Gas Dynamics, Eds. R. Brun, R. Campargue, R. Gatignol, J.C. Lengrand, Cépaduès-Éditions, Marseilles, pp. 711-718, 1998.
14. S.E. Vargo, The Development of the MEMS Knudsen Compressor as a Low Power Vacuum Pump for Portable and In Situ Instruments, Ph.D. thesis, Los Angeles, University of Southern California, Los Angeles, CA, 2000.
15. M. Young, Investigation of Several Important Phenomena Associated With the Development of Knudsen Compressors, Ph.D. thesis, University of Southern California, Los Angeles, CA, 2004.
16. Y.-L. Han, Investigation of Micro/Meso-Scale Knudsen Compressors at Low Pressures, Ph.D. thesis, University of Southern California, Los Angeles, CA, 2006.
17. O. Reynolds, On Certain Dimensional Properties of Matter in the Gaseous State, Phil. Trans. Royal Soc. London, Vol 170, pp. 727 - 845, 1880.
18. E. Graham, Phil. Trans. 1831, Phil. Trans. 1846 and 1863 (as reported by O. Reynolds Ref. 17)

19. W. Gaede, Die äußere Reibung der Gase, Annalen der Physik vol. 346(7), pp. 289-336, 1913.
20. P. Clausing, Über die Strömung sehr verdünnter Gase durch Röhren von beliebiger Länge, Annalen der Physik, vol. 404(8), pp. 961-989, 1932
21. S. Weber, W.E., Keeson, Comm. Kamerling Onnes Lab., Univ. Leiden, no. 223b, 1932; no. 246 a-d, 1936.
22. S. Chu Liang, On the Calculation of Thermal Transpiration, Canadian Journal Chemistry, vol. 33, pp. 279, 1955.
23. E.A. Mason, R.R. Evans, G.M. Watson, Gaseous Diffusion in Porous Media. III. Thermal Transpiration, Journal of Chemical Physics, vol. 38(8), pp. 1808, 1963.
24. K. Takao, in Rarefied Gas Dynamics, Ed L. Taibot, Academic Press Inc., New York, pp. 465, 1961.
25. C. Cercignani, A. Daneri, Flow of a Rarefied Gas between Two Parallel Plates, Journal of Applied Physics, vol. 34, pp. 12, 1963.
26. J.N. Ferziger, Flow of a Rarefied gas through a Cylindrical Tube, Physics of Fluids, vol. 10, pp. 1448, 1967.
27. Y. Sone, K. Yamamoto, Flow of a rarefied Gas through a Circular Pipe, Physics of Fluids, vol. 11(8), pp. 1672,1968.
28. S.K. Loyalka, Thermal Transpiration in a Cylindrical Tube, Physics of Fluids, vol. 12(11), pp.2301, 1969.
29. C. Cercignani, F. Sernagiotto, Cylindrical Poiseuille Flow of a Rarefied Gas, Physics of Fluids, vol. 9(1), pp.40, 1966.
30. G. Miller, R. Buice, On the Knudsen Limiting Law of Thermal Transpiration, Journal Physical Chemistry, vol. 70(12), pp.3874, 1966.
31. S.K. Loyalka, Kinetic Theory of Thermal Transpiration and Mechanocaloric Effect I, Journal of Chemical Physics, vol. 55(9), pp.4497, 1971.

32. S.K. Loyalka, T.S. Storvick, S.S. Lo, Thermal Transpiration and Mechanocaloric Effect IV. Flow of a Polyatomic Gas in a Cylindrical Tube, Journal of Chemical Physics, vol. 76(8), pp.4157, 1982.
33. P.E. Suetin, B.T. Porodnov, V.G. Chernjak, and S.F. Borisov, Poiseuille Flow at Arbitrary Knudsen Numbers and Tangential Momentum Accommodation, Journal of Fluid Mechanics, vol. 60(3), pp.581, 1973.
34. B.T. Porodnov, P.E. Suetin, S.F. Borisov, and V.D. Akinshin, Experimental Investigations of Rarefied Gas Flows in Different Channels, Journal of Fluid Mechanics, vol. 64(3), pp.417, 1974.
35. V. Selesnev, B. Porodnov, V. Akinshin, V. Surguchev, A. Tarin, Seperation of Binary Gas Mixtures and Their Effusion Through a Capillary and a Nuclear Filter into Vacuum, in rarefied Gas Dynamics, Eds O.M. Belotserkovskii, M.N. Kogan, S.S. Kutateladze, A.K. Hebrov, vol 2, pp. 1341,1985.
36. T. Ohwada, Y. Sone, K. Aoki, Numerical Analysis of the Poiseuille and thermal Transpiration Flow Between two Parallel Plates on the Basis of the Boltzmann Equation for Hard sphere Molecules, Physics of Fluids A, vol.1, pp. 2042, 1989.
37. Y. Sone, E. Ikatura, Analysis of Poiseuille and Thermal Transpiration Flow for Arbitrary Knudsen Numbers by a Modified Knudsen Number Expansion Method and Their Database, Journal of the Vacuum Society Japan, vol. 33(3), pp. 92, 1990. (in Japanese)
38. F.M. Sharipov, V.D. Seleznev, Rarefied Flow Through a Long Tube at any Pressure Ratio, Journal of Vacuum Science & Technology A, vol. 12(5), pp. 2933,1994.
39. F. M. Sharipov, Rarefied Gas Flow Through a Long Tube at Arbitrary Pressure and Temperature Drops, Journal of Vacuum Science & Technology A, vol. 15(4), pp. 2434, 1997.
40. F.M. Sharipov, Non-isothermal Rarefied Gas Flow through a Slit, Physics of Fluids, vol.9(6), pp.262, 1996.

41. F.M. Sharipov, Non-isothermal Gas Flow through Rectangular Microchannels, Journal of Micromechanics and Microengineering, vol. 9, pp.394-401, 1999.
42. P. Norberg, L.G. Petersson, I. Lundstrum, Characterization of gas Transport Through Micromechanical submicron Channels in Silicon, Vacuum, vol. 45, pp. 139, 1994. also I. Lundstrum, P. Norberg, L.G. Petersson, Wall Induced Effects on Gas Transport Through Micromechanical Channels in Silicon, Journal of Applied Physics, vol. 76(1), pp.142, 1994.
43. E.R. Arkilic, M.A. Schmidt, K.S. Breuer, TMAC measurements in Silicon Micromachined Channels, in rarefied Gas Dynamics, Ed Ching Shen, pp. 983, 1995.
44. J.L. Spencer, L.F. Brown, Experimental Observation of Gas Phase-Adsorbed Phase Interactions During Counter diffusion in Porous Alumina, Journal of Chemical Physics, vol. 63(7), pp.2882, 1975.
45. V.D. Borman, S. Yu. Krylov, A.V. Prosyanov, A.M. Kharitonov, Theory of Transport Processes in Nonequilibrium Gas-Solid Systems, Soviet physics, JETP, vol. 63(1), pp. 43,1986.
46. V.D. Borman, S. Yu. Krylov, A.V. Prosyanov, Theory of Nonequilibrium Phenomena of a Gas-Solid Interface, Soviet physics, JETP, vol. 67(10), pp. 2110, 1988.
47. V.D. Borman, S. Yu. Krylov, A.V. Prosyanov, Fundamental Role of Unbound Surface Particles in Transport Phenomena along a Gas-Solid Interface, Soviet physics, JETP, vol. 70(6), pp. 1013, 1990.
48. R.M. Hoogeveen, L.J.F. Hermans, V.D. Borman, S. Yu. Krylov, Unified Description of Rotating-Molecule-Surface Interaction: Comparison with Experiment, Physical Review A, vol. 42(11), pp.6480, 1990.
49. J.J.M. Beenakker, V.D. Borman, S. Yu. Krylov, Molecular Transport in the Nanometer Regime, Physical Review Letters., vol. 72(4), pp. 514,1994.
50. J.J.M. Beenakker, V.D. Borman, S. Yu. Krylov, Molecular Transport in Subnanometer Pores: Zero-Point Energy, Reduced Dimensionality, and Quantum Sieving, Chemical Physics Letters, vol. 232, pp.379, 1995.

51. V.I. Roldughin, V.M. Zhdanov, Effect of Surface Forces on the Gas Flow in Nanosize Capillaries, in rarefied Gas Dynamics, Ed. M. Capillaries, AIP Conference Proceedings, vol. 762, pp. 774, 2005.
52. S.V. Nader, A.J.H., Frijns, A.A. van Stennnhoven, A.J. Markvoort, P.A.J. Hilbers, Hybrid Molecular Dynamic- Mote Carlo Simulation for the Properties of a Dense and Dilute Gas in a Microchannel, in rarefied Gas Dynamics, Ed. M. Capillaries, AIP Conference Proceedings, vol.767, pp. 774, 2005.
53. http://eande.lbl.gov/ECS/aerogels/satcond.htm
54. B.T. Porodnov, A.N. Kulev, F.T. Tuchvetov, Thermal Transportation in a Circular Capillary with a Small Temperature Difference, Journal of Fluid Mechanics, vol. 88(4), pp.609-622, 1978.
55. W. Crookes, On attraction and Repulsion from Radiation, Proceedings of the Royal Society A, vol. 23, pp. 373, 1875.
56. O. Reynolds, On the Force Caused by the Communication of Heat between a Surface and a Gas; and on a new Photometer, Philosophical Transactions of the Royal Society A, vol. 166, pp. 725, 1876.
57. Maxwell, J.C., On Stresses in Rarefied Gases arising from Inequalities of Temperature. Philosophical Transactions of the Royal Society A, vol. 170, pp. 231-256, 1879.
58. H.E. Marsh, E. London, L.B. Loeb, The Theory of the Radiometer, Journal of the Optical Society of America, pp. 257, 1925.
59. M. Kogan, V.S. Galkin, O.G. Fridlander, Stresses Produced in Gases by Temperature and Concentration Inhomogeneities. New Types of Free Convection, Soviet physics, Uspekhi, vol. 19, pp. 420, 1976.
60. K. Aoki, Y. Sone, N. Misukawa, A Rarefied Gas Flow Induced by a Temperature Field, in Rarefied Gas Dynamics, Eds. J. Harvey, G. Lord, Oxford University Press, Oxford, pp.35, 1995.

61. D.C Wadsworth, E. P. Muntz, G. Pham-Van-Diep, P. Keeley, A Micromechanical Knudsen Compressor, Rarefied Gas Dynamics, Eds. J. Harvey and G Lord, Oxford University Press, Oxford, pp. 708-714, 1995.
62. M. Ota, K. Kawata, Direct Simulation of Gas Flows around rarefied Gas Dynamics Engines for a Micro-Machine, in rarefied Gas Dynamics, Eds. J. Harvey and G Lord, Oxford University Press, Oxford, pp. 722, 1995.
63. M. Ota, T. Nabu, M. Sakamoto, Numerical Simulation of Molecular Motion around Laser Microengine blades, Mathematics and Computers in Simulations, vol. 55, pp. 223, 2001.
64. K. Aoki, S. Takata, H. Aikawa, F. Goise, A rarefied Gas Flow Caused by a Discontinuous Wall Temperature, Physics of Fluids, vol. 13(9), pp. 2645, 2001.
65. Y. Sone, Y. Wanigachi, K. Aoki, One-way Flow of a rarefied Gas Induced in a Channel with Periodic Temperature Distribution, Physics of Fluids, vol. 8, pp. 2227, 1996.
66. G. A. Bird, Molecular Gas Dynamics and the Direct Simulation of Gas Flows, Oxford Science Publications, Oxford, 1994.
67. Alexeenko, S.F. Gimelshein, E.P. Muntz, A.D. Ketsdever, Kinetic Modeling of Temperature Driven Flows in Short Microchannels, International Journal of Thermal Science, in press, 2006.

Figures

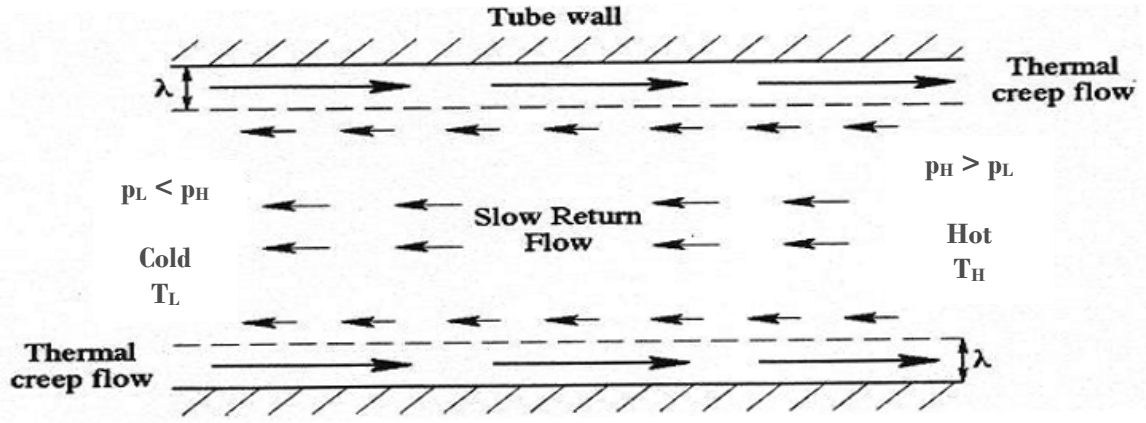

Figure 1: Illustration of Knudsen's view of the thermal creep flow[7,8]

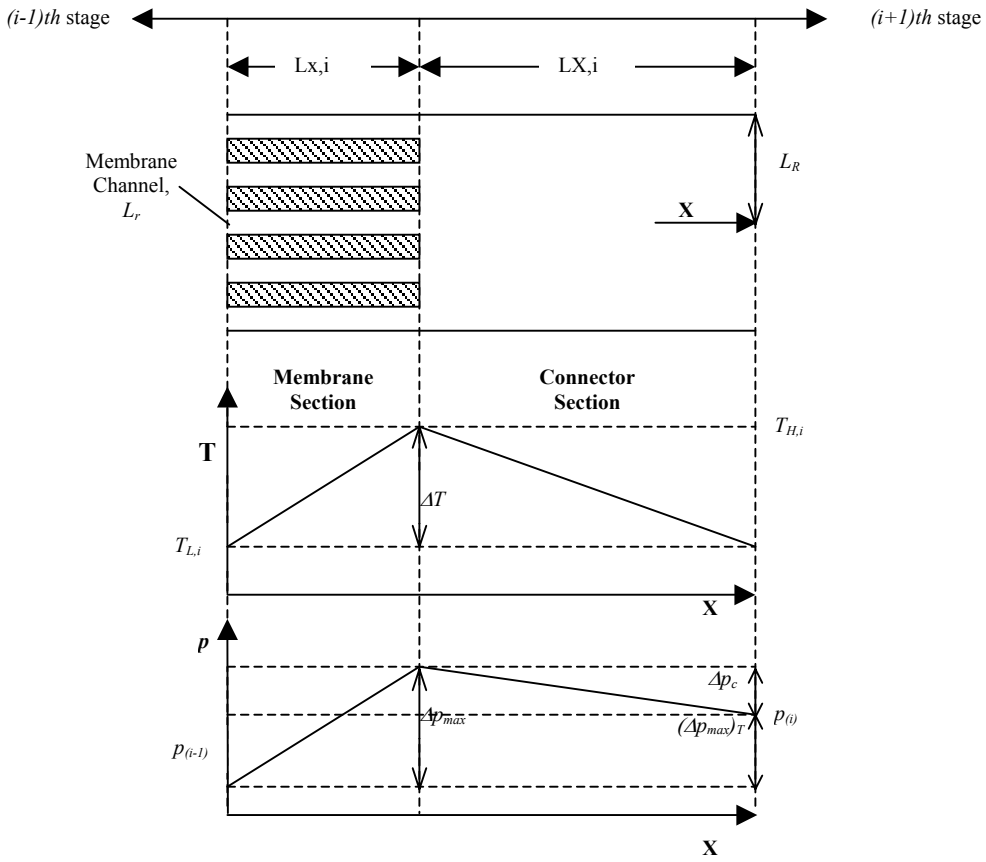

Figure 2: Illustrative i[th] stage of a Knudsen Compressor[12]

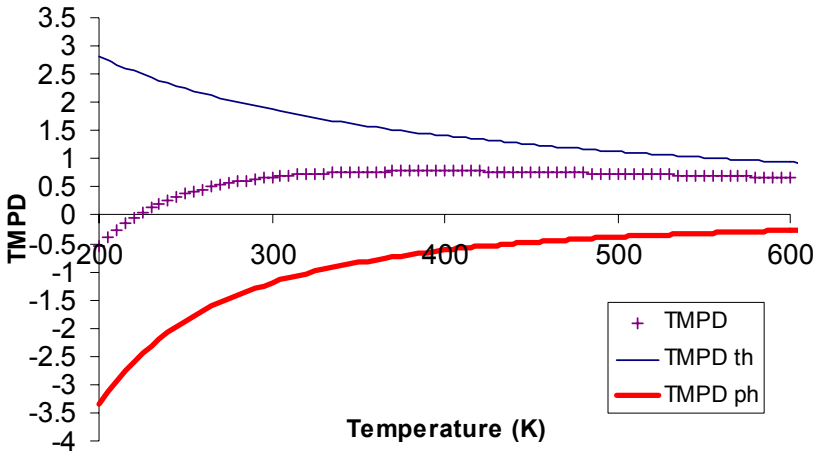

Figure 3: Gas-phonon coupling driven flow for CO_2 on C[15]

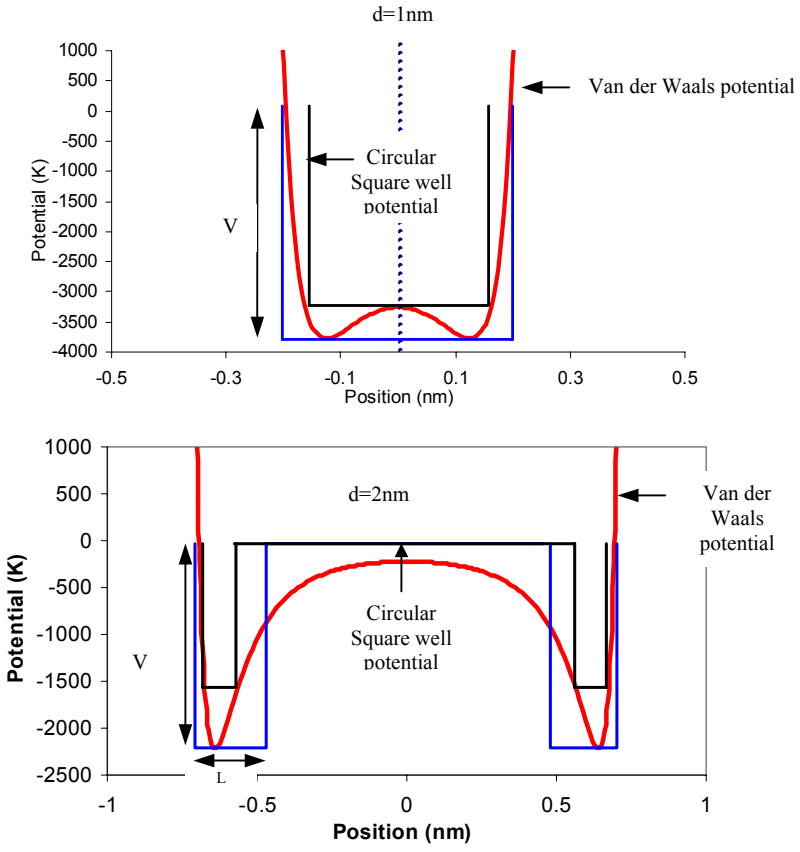

Figure 4: Nano-scale circular channel potential models[15]

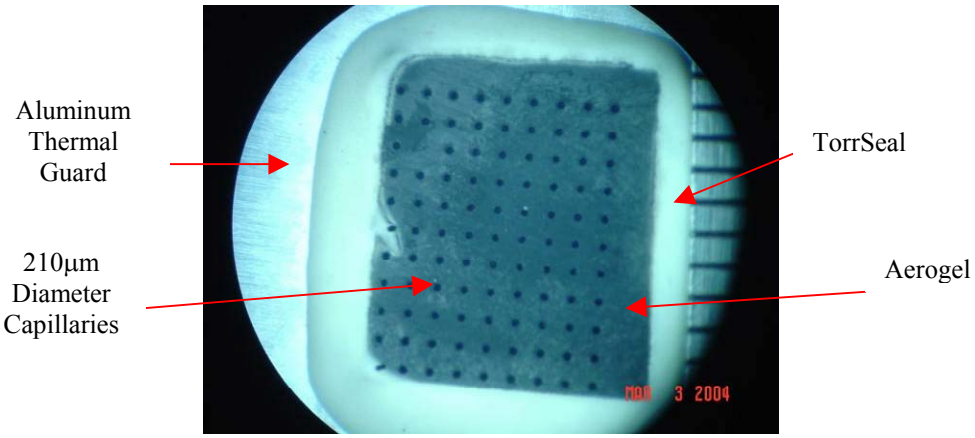

Figure 5: Image of the mechanically machined Aerogel membrane with capillaries

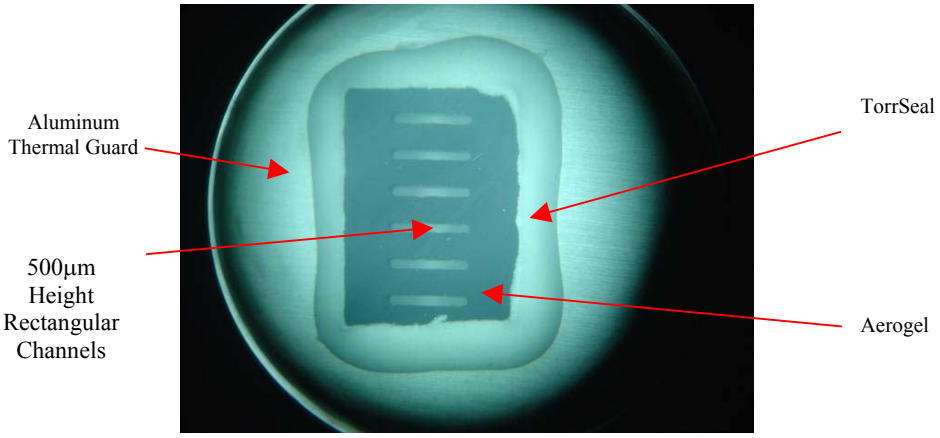

Figure 6: Image of the mechanically machined Aerogel membrane with rectangular channels

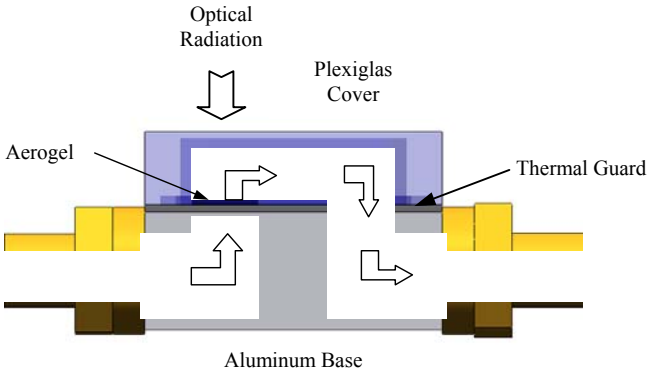

Figure 7: Cross-section of the single stage Knudsen Compressor

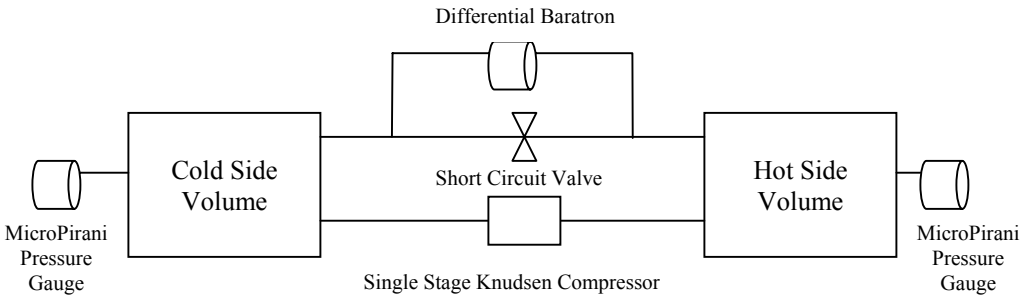

Figure 8: Schematic of the experimental setup

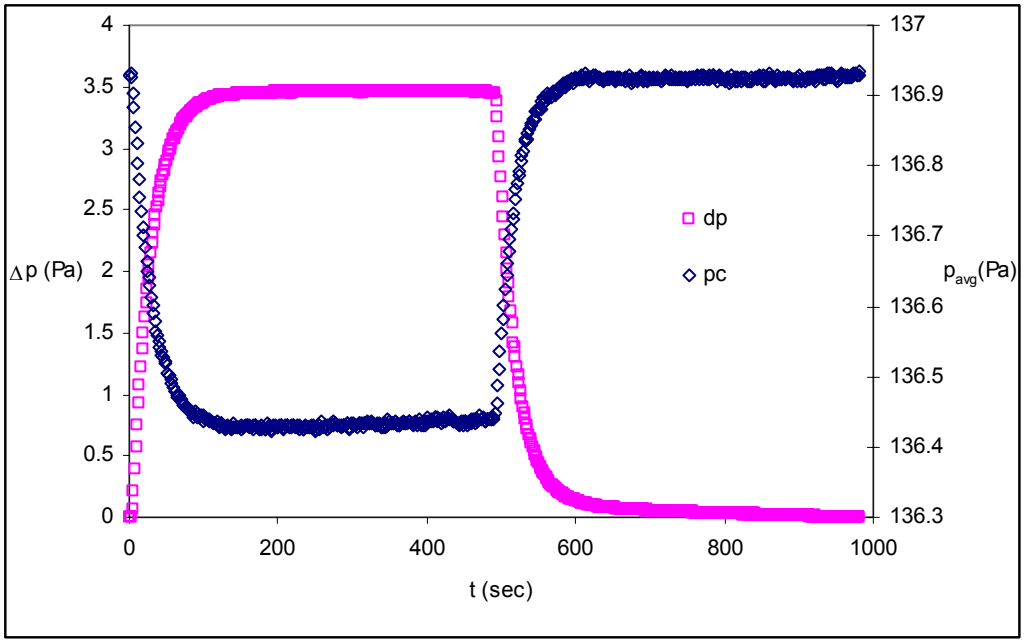

Figure 9: Time trace of the mechanically machined aerogel membrane with 210 μm diameter capillaries at an operating pressure of around 136 Pa

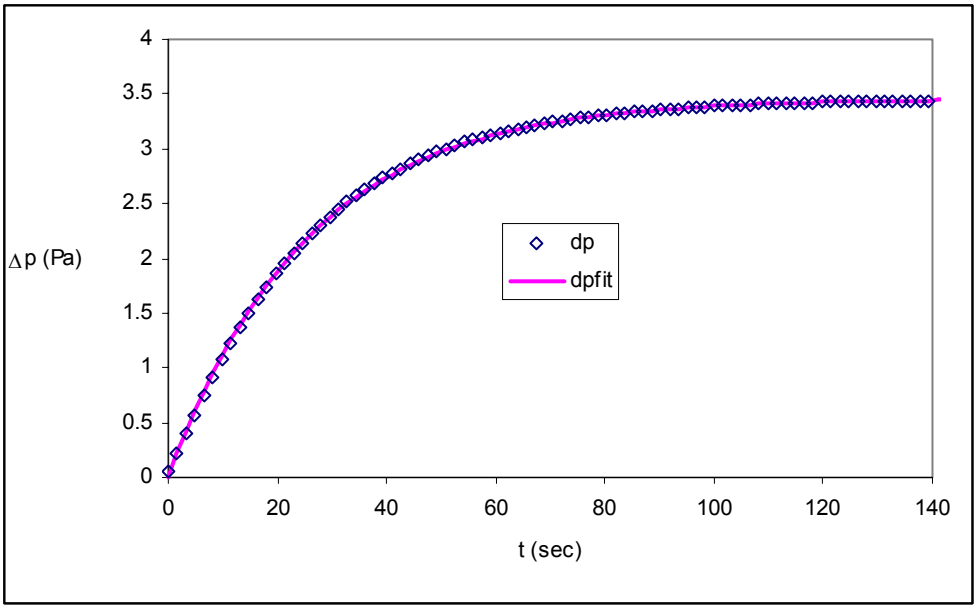

Figure 10: Curve fit of the time trace of 210 μm diameter capillary membrane at an operating pressure of around 136 Pa

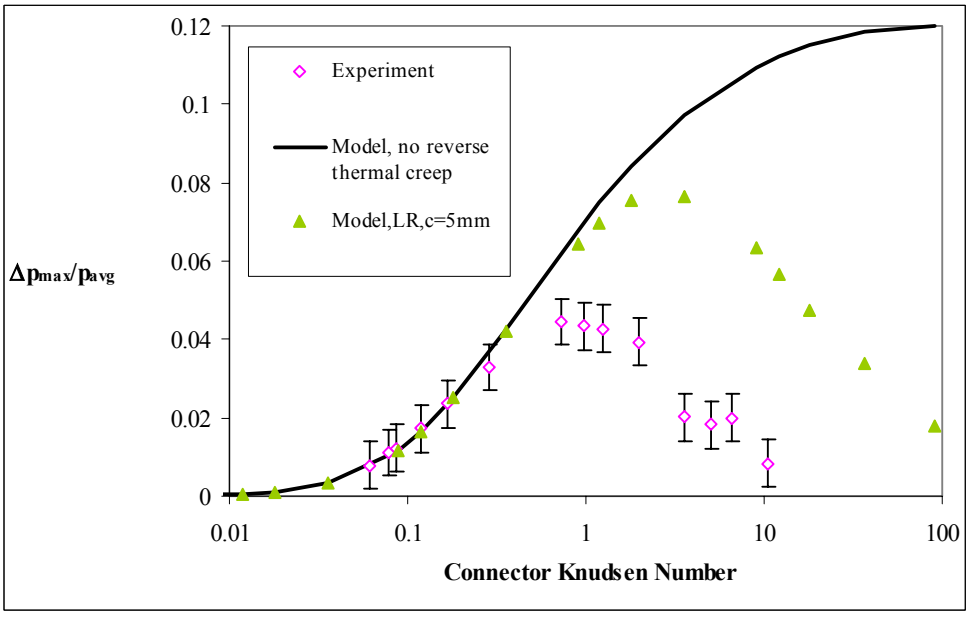

Figure 11: Comparison of the $\Delta p_{max}/p_{avg}$ (380 μm capillaries membrane)

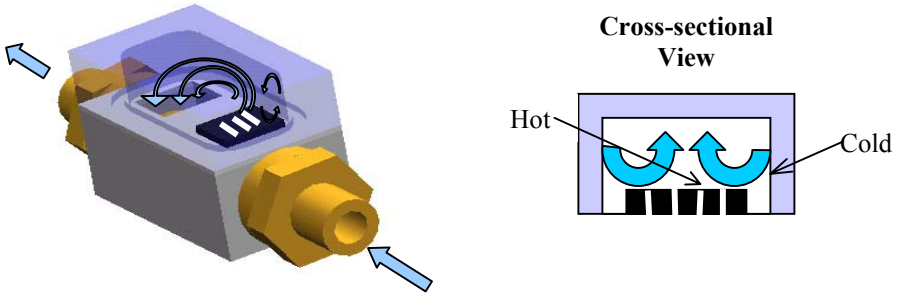

Figure 12: Possible flow pattern of thermally induced internal circulation

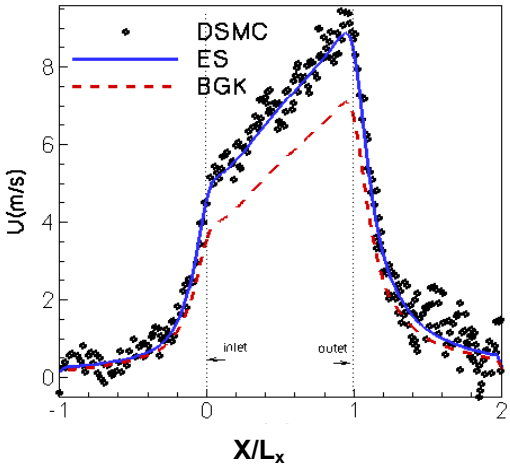

Figure 13: X-component of velocity along the channel centerline obtained by DSMC, ES and BGK models $Kn_{h/2}$= 1.

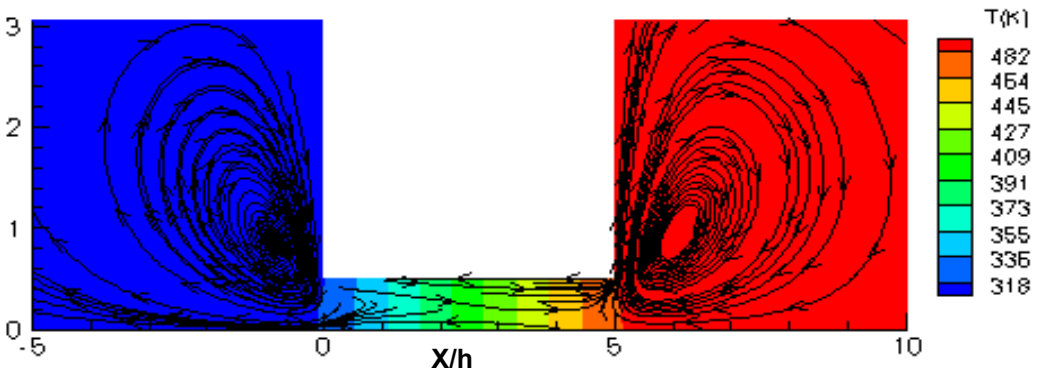

Figure 14: Temperature contours and streamlines for thermal creep flow in a 2D channel: Lx/h=5, T_L=300 K, T_H=500 K, $Kn_{h/2}$= 1, $Kn_{H/2}$=0.2.

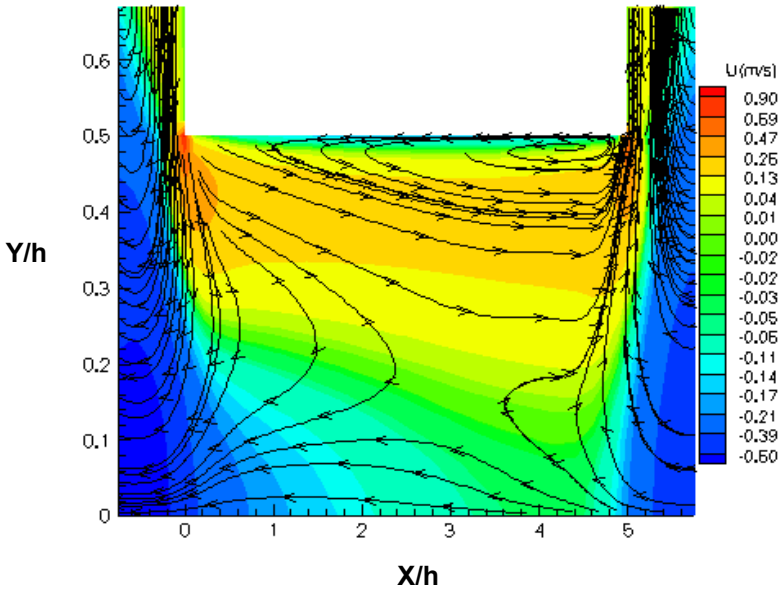

Figure 15: X-component of velocity contours and streamlines (zoom) for thermal creep flow in a 2D channel: Lx/h=5, T_L=300 K, T_H=500 K, $Kn_{h/2}$= 1, $Kn_{H/2}$=0.2.

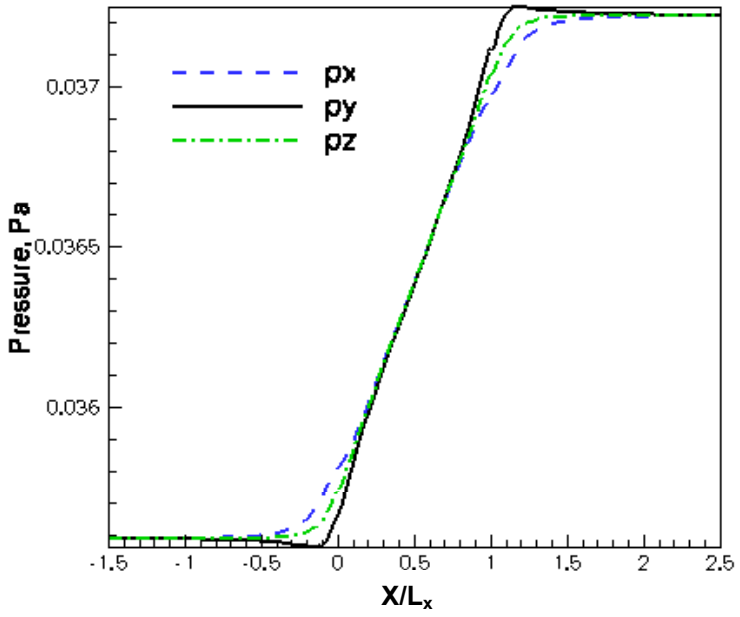

Figure 16: Pressure tensor components along the centerline of the channel for thermal creep flow at Lx/h=5, T_L=300 K, T_H=500 K, $Kn_{h/2}$= 1, $Kn_{H/2}$=0.2.

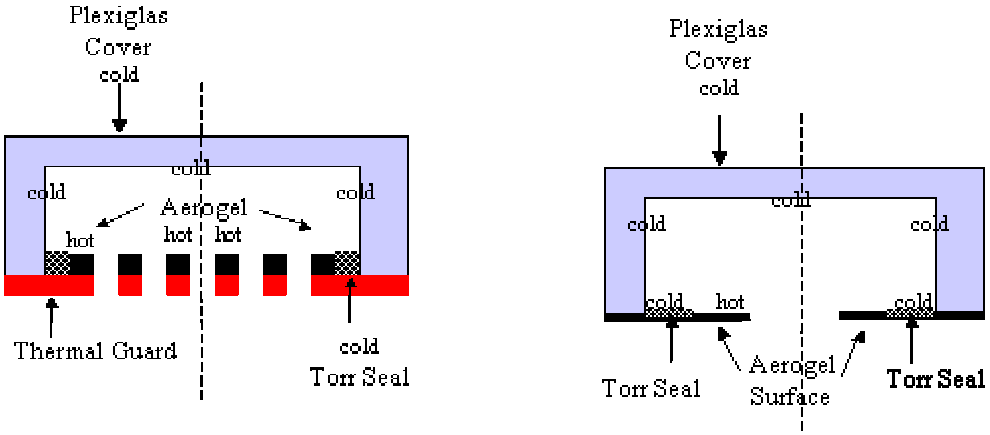

Figure 17: (a) Cross-sectional view of the current single stage design (b) Simulation stage mimicking the current single stage design

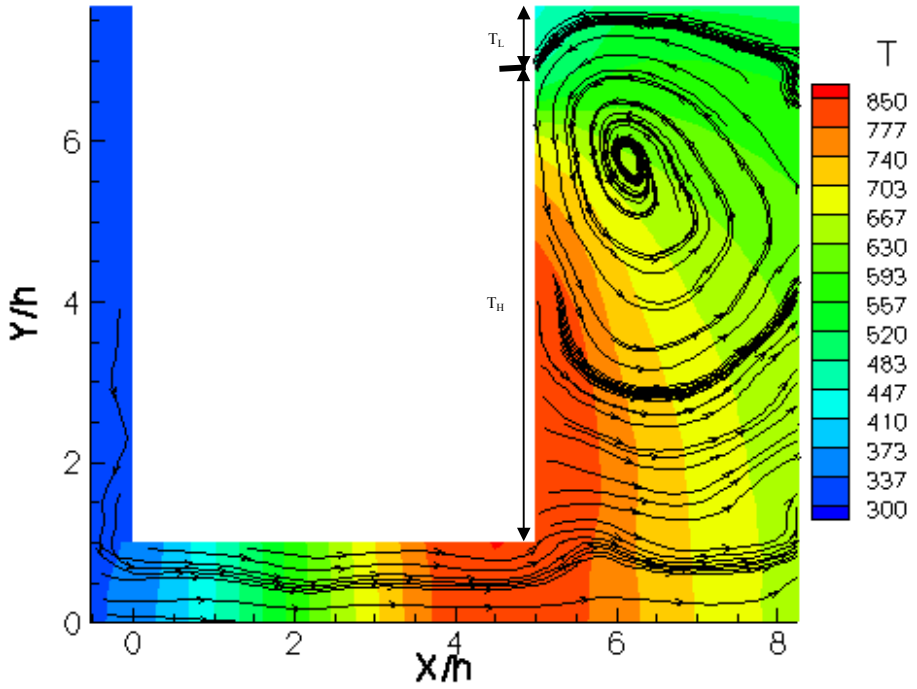

Figure 18: Temperature contours and streamlines for DSMC simulation case mimicking the current single stage design: Lx/h=5, T_L=300 K, T_H=1000 K, $Kn_{h/2}$= 2.7, $Kn_{H/2}$=0.3.